Research Article   **Open Access**

Accumulation and Distribution of Non-targeted and Anti-CD44-conjugated Quantum Dots in Distinct Phenotypes of Breast Cancer

Simona Steponkiene[1], Dominyka Dapkute[1], Una Riekstina[2] and Ricardas Rotomskis[1,3]*

[1]*Biomedical Physics Laboratory, National Cancer Institute, P. Baublio 3b, 08406, Vilnius, Lithuania*
[2]*Medicine Faculty, University of Latvia, 19 Raina blvd., LV-1586, Riga, Latvia*
[3]*Biophotonics Group of Laser Research Center, Vilnius University, Sauletekio 9, 3rd building, 10222, Vilnius, Lithuania*

Abstract

Background: It has been postulated that most if not all cancers are hierarchically organized and contain distinct phenotypes of cells. In breast tumors $CD44^+/CD24^-/EpCAM^+$ phenotype had been shown to possess the properties of cancer stem-like cells, while $CD44low/^-/CD24^+/EpCAM^+$ cells represent more differentiated tumor cells that are often classified as luminal subtype of cancer. Quantum dots had already been used for imaging *in vitro* and *in vivo*, however the information about accumulation and time-dependent distribution of antibody-conjugated quantum dots in different phenotypes of breast cancer is still missing.

Results: The accumulation and distribution of QDs was compared between $CD44low/^-/CD24^+/EpCAM^+$ (MCF-7) and $CD44^+/CD24^-/EpCam^+$ (MDA-MB-231) cells. The accumulation of non-targeted QDs was twofold more efficient in $CD44low/^-/CD24^+/EpCAM^+$ cells than in $CD44^+/CD24^-/EpCam^+$. Conjugation of anti-CD44 to QDs minimized uptake of QDs in $CD44low/^-/CD24^+/EpCAM^+$ cells thus showing the selectivity of this conjugate to CD44-positive cells. Most importantly, after 24 hours post labeling the membrane-bound anti-CD44-QDs was engulfed inside the cytoplasm of cells, while the conjugate of anti-CD44 and fluorescein isothiocyanate (FITC) remained on the cell membrane.

Conclusion: The combination of QDs and antibodies gives a synergistic effect; antibody assures specific labeling of the desired cells while QDs initiate engulfment of the conjugate inside cells. Antibodies themselves are not capable of initiation of receptor-mediated endocytosis. Therefore these results are very important and might be used in the development of multifunctional agents for targeted labeling and delivery of bioactive compounds.

Introduction

Increasing number of reports postulate that there is a subpopulation within tumors which share properties of stemness: possess an unlimited capacity to proliferate, self-renew, and differentiate in order to sustain tumor growth and progression, but most importantly these cancer cells are more likely to survive conventional chemotherapy and radiotherapy [1-3]. Scientists are working on the identification of molecular markers which could be used to selectively detect the phenotype of these aggressive cells and eliminate their population, thus stopping the progression of the cancer as well as metastasis [4-6]. CD44 is a transmembrane glycoprotein which is reported to regulate growth, survival, differentiation, migration, tumor progression and metastasis [7]. Labeling of cancer stem-like cells by a combination of CD44 and CD24 markers was firstly reported in breast cancer [8]. Later CD44 marker was also approved for prostate [9], pancreatic [10], colon [11] and other types of cancer [12], thus showing its significance in the development of targeted anti-cancer therapies.

Advances in nanotechnology have contributed to the development of novel nanoparticles that enable the tumor-specific delivery of imaging probes and therapeutic agents. There have already been attempts to use anti-CD44 in construction of a tool for nanotechnology-based detection and eradication of stem-like cancer cells. Wang et al. demonstrated the selective accumulation of anti-CD44-conjugated liposomal nanoparticles in hepatocellular carcinoma *in vivo* [13]. Numerous studies used hyaluronic acid and nanoparticle conjugates to achieve the targeting of $CD44^+$ cancer stem-like cells [14-16].

Recently, it was suggested that multifunctional nanoparticles hold a great promise for the future of cancer treatment because they combine tumor-targeted imaging and therapy in an all-in-one system [17]. Quantum dots (QDs) have gained much attention due to unique optical and electronic properties: emission from visible to infrared wavelengths, large absorption coefficients across a wide spectral range, and very high levels of brightness and photostability [18,19]. The surface chemistry of QDs allows conjugation of the bioactive molecules (antibodies, etc.) and various therapy agents including chemotherapeutic drugs or photosensitizers [20-22]. Peptide- and antibody-coated QDs have already been reported to selectively detect cancer cells *in vivo* [23,24]. However, the information about accumulation dynamics, localization, and time-dependent distribution of non-targeted and anti-CD44-conjugated quantum dots in different phenotypes of cancer cells is still limited.

In this study we used eFluor® 605NC to investigate the accumulation dynamics and distribution of non-targeted and anti-CD44-conjugated QDs in $CD44^{low/-}/CD24^+/EpCAM^+$ (MCF-7) and $CD44^+/CD24^-/EpCam^+$ (MDA-MB-231) cells. Non-targeted QDs accumulated in both types of cells but the photoluminescence (PL) intensity of

*Corresponding author: Ricardas Rotomskis, Biophotonics Group of Laser Research Center, Vilnius University, Sauletekio 9, 3rd building, 10222, Vilnius, Lithuania, Tel: +37052190908; E-mail: ricardas.rotomskis@ff.vu.lt

quantum dots per cell was higher in MCF-7. Anti-CD44-QDs allowed to minimize labeling of CD44$^{low/-}$ cells and thus to achieve selectivity to cancer stem-like CD44$^+$ cells. Most importantly, the anti-CD44-QDs conjugate was engulfed within 24 hours inside the cells, demonstrating the ability of QDs to deliver molecular cargo into the cytoplasm of cells.

Materials and Methods

Materials

Human breast cancer cell lines MDA-MB-231 and MCF-7 were obtained from the American Type Culture Collection (ATCC HTB-26™; ATCC HTB-22™). Doxorubicin was obtained from Teva Pharmaceutical Industries (Lithuania). Two types of QDs were purchased from eBioscience (USA): non-targeted carboxyl coated eFluor® 605NC and anti-CD44-conjugated eFluor® 605NC. Both QDs consisted of CdSe/ZnS core/shell and were coated by functionalized PEG lipids [25]. The diameter of eFluor® 605NC was 22 nm and zeta potential was -12 mV [26]. The mouse anti-human CD44 monoclonal antibodies conjugated with fluorescein isothiocyanate (FITC) (Sigma-Aldrich, USA), anti-human CD24 conjugated with phycoerythrin (PE) (eBioscience, USA) and anti-human EpCAM conjugated with allophycocyanin (APC) (Miltenyi Biotec, Germany) were used. Crystal violet for fixed colonies staining was obtained from Alfa Aesar (USA). The cell proliferation kit (XTT) was purchased from Biological Industries (Israel).

Cell culture

MCF-7 and MDA-MB-231 cells were cultured in Dulbecco Modified Eagle's Medium (Biochrom, Germany), supplemented with 10% fetal bovine serum (Gibco, USA), 100 U/ml penicillin, 100 mg/ml streptomycin (Biochrom, Germany) and 4 mM L-Alanyl-L-Glutamine (Biochrom, Germany). Cells were cultured and passaged in 25 cm² cell culture flasks with up to 90% confluence with complete cell culture medium in a humidified chamber at 37°C with 5% CO_2.

Laser scanning confocal microscopy

Samples were examined under the Nikon Eclipse TE2000-S, C1si confocal microscope (Nikon, Japan) by scanning with the beam of UV laser (404 nm) for Hoechst, argon ion laser (488 nm) for Alexa Fluor®488 and FITC, and helium-neon laser (543 nm) for QDs using oil immersion 60× NA 1.4 objective (Plan Apo VC, Nikon, Japan). Fluorescence of Hoechst was detected using 450/35 band pass filter. To visualize Alexa Fluor®488 and FITC, the band pass filter 515/30 was used. QDs fluorescence was detected by a 605/75 band pass filter. The 32-channel spectral detector was used to investigate PL of QD in a single cell. Images were captured and processed with EZ-C1 3.90 image analysis software (Nikon Instruments, USA) and Image J 1.48 (National Institute of Health, USA) software.

Flow cytometry

Flow cytometric analyses were performed by Accuri C6 (Becton Dickinson, USA) or LSR II (Becton Dickinson, USA) flow cytometers. A minimum of 10000 viable cells were measured per sample. The data were analyzed with Flow Jo (Tree Star, USA) or Accuri C6 software.

Phenotypic analysis of MCF-7 and MDA-MB-231 cells

For flow cytometry analysis, 1×10^6 cells were trypsinized, pelleted by centrifugation at 200 g for 7 minutes and resuspended in a final 100 μL volume of phosphate buffered saline (PBS) solution containing 20 μL antibody (anti-CD44, anti-CD24, anti-EpCam) stock solution. Cells were incubated for 20 min at 4°C, washed and analyzed with a flow cytometer.

Colony forming efficiency

For colony formation assay, cells were seeded in a 6-well plate at a density of 400 viable cells per well in triplicate and kept for 10 days in the incubator under standard conditions. After colonies had been formed, cells were fixed using ascending series of ethanol (70%, then 96%, 10 min each) and stained with 0.05% crystal violet. Colonies were imaged using a microscope (Nikon Eclipse TE2000-U, Japan; camera Leica DFC290, Germany). Only colonies with more than 40 cells were counted. Colony forming efficiency (CFE) was determined by the following formula (1):

$$CFE\,(\%) = \text{Colonies Counted/Cells Seeded} \times 100 \qquad (1)$$

Cytotoxicity studies

To compare chemoresistance, MDA-MB-231 and MCF-7 cells were seeded in a 96-well plate at a density of 9000 cells per well and cultured for 24 hours. The chemotherapeutic drug doxorubicin was diluted in a complete growth medium to final concentrations of 2.7-500 ng/ml and added to the cells. Cells were maintained continuously in doxorubicin for 72 hours. For viability assessment cells were treated with an activated-XTT solution and after 2-4 hours the absorbance was measured using BioTek (USA) plate reader at a wavelength of 490 nm. The absorbance of the sample was expressed mathematically as follows (2):

$$Absorbance = A_{490}\,(test) - A_{490}\,(blank); \qquad (2)$$

Where A_{490} (blank) – the absorbance of a solution in the cell-free well

To test the influence of QDs on cell viability cells were seeded in a 12-well plate at a density of 40 000 cells per well and cultured for 24 hours. QDs were diluted to the concentration of 5 x 10^{-8} M and added to the cells. After 3-72 hours incubation the cells were trypsinized, centrifuged (7 min, 200 g) and resuspended in 200 μl PBS. 20 μl of cell suspension were mixed with the equal amount of AccuStain Solution T (Nano Entek, Korea), which contains propidium iodide (PI) and lysis solution, therefore provides the total number of cells, or AccuStain Solution N (Nano Entek, Korea), which contains only PI in PBS and gives the number of dead cells. Stained cell suspensions were loaded onto plastic chips and inserted into the automated cell counter ADAM (Nano Entek, Korea) which counts the cells and calculates their viability.

Accumulation of non-targeted quantum dots

MCF-7 and MDA-MB-231 cells were seeded in the 8-well glass chamber slide (Nunc Lab-Tek II, Thermo Fisher Scientific, USA) at a density of 100000 cells/well. The cells were allowed to grow for 24 hours before the addition of QDs. Non-targeted QDs were diluted to a concentration of 5 x 10^{-8} M in the complete growth medium and poured over the MCF-7 and MDA-MB-231 cells. After 3-24 h incubation with QDs at 37°C the cells were washed with Dulbecco's phosphate buffered saline (DPBS) (supplemented with Ca^{2+} and Mg^{2+} to prevent cell detachment) (Biochrom, Germany) to remove any excess QDs. Then cells were fixed with 4% paraformaldehyde (PFA) (Sigma-Aldrich, USA) for 15 min, permeabilized for 4 min using 0.2% Triton X-100 (Sigma-Aldrich, USA) and blocked for 20 min with PBS containing 1% bovine serum albumin (BSA) (Sigma-Aldrich, USA). To label actin, fixed and BSA-blocked cells were incubated with 5U/ml Alexa Fluor®488 Phalloidin (Life Technologies, USA) methanolic solution for 20 min. Before mounting the slides with Qdot® Mounting media (Life Technologies, USA), the nuclei were stained with 25 μg/ml

Hoechst 33258 (Sigma-Aldrich, USA) for 30 min.

Quantification of non-targeted quantum dots accumulation

To determine the fluorescence intensity of QDs inside a single cell, MCF-7 and MDA-MB-231 cells were seeded in a 12-well plate at a density of 40 000 cells per well and cultured for 24 hours. Non-targeted QDs were diluted to the concentration of 5×10^{-8} M and poured over the cells. After 3-72 hours incubation the cells were trypsinized, washed by centrifugation (7 min, 200 g) and suspended in 100 µl PBS. Their fluorescence intensity was determined by flow cytometry.

To test the differences between the uptake of QDs and fluorescent chemotherapeutic drug doxorubicin, both cell lines were seeded in a 12-well plate at a density of 40 000 cells per well and after 24 hours were continuously incubated with 65 ng/ml doxorubicin. After 3-72 hours the cells were trypsinized and analyzed using flow cytometry.

Accumulation of anti-CD44-conjugated quantum dots

MCF-7 and MDA-MB-231 cells were seeded in the 8-well glass chamber slide (Nunc Lab-Tek, Thermo Fisher Scientific, USA) at a density of 100 000 cells/well. After 24 hours the medium was aspirated, 100 µl of DPBS solution containing 20 µL of anti-CD44-QDs or anti-CD44-FITC were poured over the cells for 30 min. Afterwards, the cells were washed 3 times with DPBS to remove any excess antibodies and filled with fresh medium. Nuclei of the cells were stained by 30 min incubation with 25 µg/ml Hoechst 33258. Live-cell imaging was performed at two time points: immediately after labeling and 24 hours after labeling. Between measurements cells were kept in the incubator under standard culture conditions (37°C, 5% CO_2).

Statistical analysis

Data are shown as the representative result or as mean of at least three independent experiments ± SD. Statistical analyses were performed using the two-tailed Student's t test; differences were considered significant at $p < 0.05$.

Results

Characterization of cancer cells in human breast cancer cell lines

Numerous studies show that $CD44^+/CD24^-/EpCAM^+$ cells exhibit properties of cancer stem-like cells [8,27,28]. The expression of CD24, CD44 and EpCAM surface antigens was measured to define the phenotype of MDA-MB-231 and MCF-7 breast cancer cells. The flow cytometry results revealed that 100% of MDA-MB-231 cells expressed CD44 marker while the expression of CD24 was very low (~2%) (Figure 1A). In contrast to MDA-MB-231, MCF-7 cells exhibited high expression of CD24 (94%) and low expression of CD44 (11 %). EpCAM was expressed in both cell lines.

Effective colony formation (plating efficiency) shows the capability of cells to create a population from one cell [29-31]. Plating efficiency method revealed that MDA-MB-231 cells form colonies 2 times better than MCF-7 cells (~ 26% and ~ 12% respectively) (Figure 1B).

Chemoresistance is one of the major clinical criterions to characterize cancer stem-like cells [32]. To determine the sensitivity of MDA-MB-231 and MCF-7 cells to chemotherapy, we treated cells with various concentrations of doxorubicin. The IC50 value of MDA-MB-231 cells was ~ 2 times higher than MCF-7 (Figure 1C), indicating

that MDA-MB-231 cells were more resistant to the chemotherapeutic treatment.

Furthermore, we examined the morphology of MCF-7 and MDA-MB-231 cells. MDA-MB-231 cells possessed mesenchymal morphology while MCF-7 cells were epithelial-like cells (Figure 1B). Epithelial and mesenchymal cells differ in phenotype as well as function. Epithelial cells lack migratory properties, while mesenchymal cells are associated with enhanced migration, invasiveness, intra- and extravasation [33].

To sum up, we had chosen MDA-MB-231 cells as a model for $CD44^+/CD24^-/EpCAM^+$ cells, which are known for poor prognosis and are highly enriched with cancer stem-like cells [34]. MCF-7 cells served as a model for $CD44^{low/-}/CD24^+/EpCAM^+$ cells, which are less malignant cells, more sensitive to chemotherapy treatment and known for good prognosis after treatment. We further examined accumulation dynamics and distribution of non-targeted and anti-CD44-conjugated QDs in cancer cells of these distinct phenotypes.

Accumulation and distribution of non-targeted QDs

Confocal fluorescence microscopy images taken at 3, 6 and 24 hours after the incubation with QDs at 37°C showed that the localization and distribution of QDs is similar in both cell types and generally follows the accepted stages of the accumulation scheme [35-37]: after 3 hours vesicles were distributed all along the cell (Figures 2A and 2D), after 6 hours vesicles of QDs localized in close proximity to the nucleus (Figures 2B and 2E), and after 24 h, big-sized vesicular structures with QDs were formed (Figures 2C and 2F).

To determine whether any differences in QDs uptake can be registered between MCF-7 and MDA-MB-231 cells, the quantitative analysis of the diameter of vesicles was performed. As can be seen in the Figure 2G, MDA-MB-231 cells formed over 2 times larger vesicles than MCF-7 cells, and the diameter of vesicles varied within the same cell (Figures 2A-2C inserts). MCF-7 cells formed vesicles of a uniform size (Figures 2D-2F inserts), and the diameter of vesicles increased in a time-dependent manner.

Quantitative analysis revealed that PL intensity of QDs within one cell, obtained by flow cytometry, was ~ 2.4 times lower in MDA-MB-231 than in MCF-7 cells (Figure 3A). Similar trend was observed by analyzing the PL intensity of doxorubicin within one cell (Figure 3B). Such results are rather cell-type related than cell-size related, because the ratio of cell diameters of MDA-MB-231 and MCF-7 was only 1.1 (Figure 3C).

Both cancer cell lines reached saturation phase of accumulation after 48 h incubation with QDs (Figure 3A). The saturation phase might show the lack of receptors and/or caveolin for endocytosis as these molecules must be recycled back to the plasma membrane, which takes time and lengthens the internalization rate [35,36,38]. The viability of MCF-7 and MDA-MB-231 cells did not change even after the longest period of incubation with QDs (Figures 4A and 4B).

Accumulation and distribution of anti-CD44-QD conjugate

The labeling of human breast cancer cells with non-targeted QDs revealed that better uptake is seen in the MCF-7 than in MDA-MB-231 cancer cells (Figure 2). To achieve a better selectivity to MDA-MB-231, which was shown to represent a more malignant phenotype of cancer (Figure 1), cells were labeled with anti-CD44-QDs conjugate. Anti-CD44-FITC was used as a control.

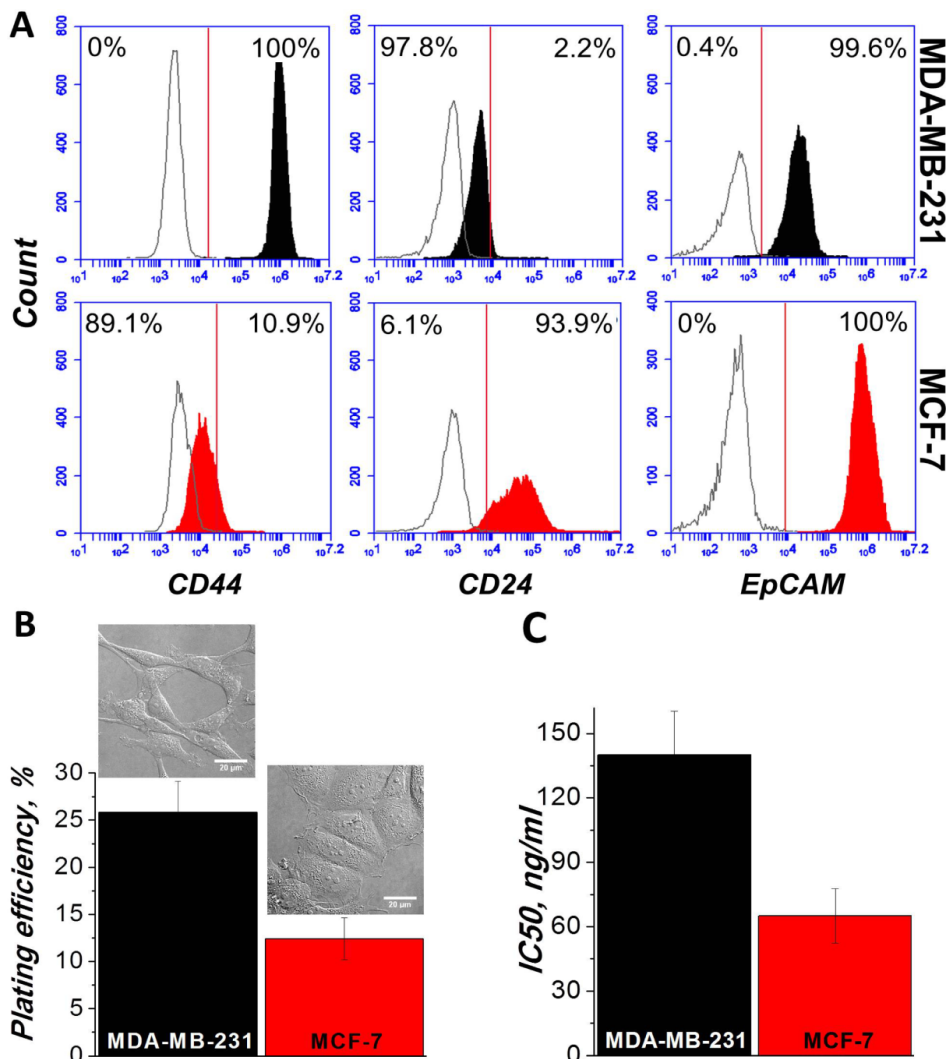As can be seen in the Figure 5A, after 30 min incubation only a

Figure 1: Phenotypical profile of MCF-7 and MDA-MB-231 breast cancer cell lines. A) Expression of CD24, EpCAM and CD44 was determined by flow cytometry.B) Plating efficiency assay was performed by seeding 400 cells per well in a 6-well plate. After 10 days of growth the colonies of >40 cells were calculated. Differential interference contrast microscopy images were taken at 24 h post seeding of untreated cells (600×). C) Response to the treatment of chemotherapeutic drug doxorubicin was obtained by seeding the cells into 96-well plate and giving different concentrations of doxorubicin for 72 h. Viability and proliferation was measured by XTT assay. IC50 value shows the concentration of doxorubicin which reduces the number of viable cells twice.
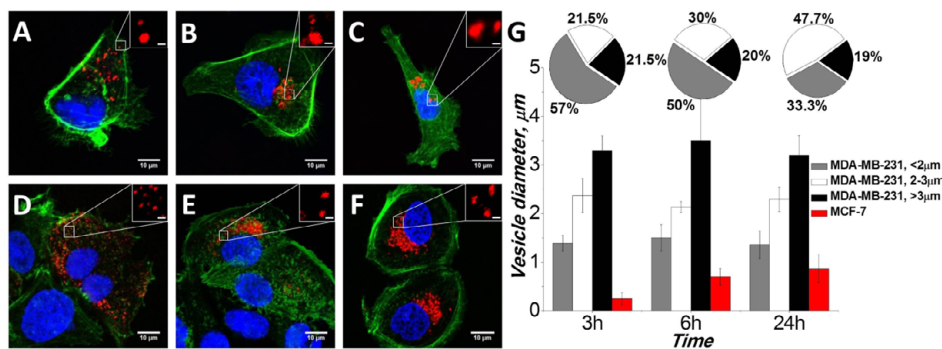

Figure 2: Uptake of non-targeted QDs in breast cancer cells. Fluorescence confocal micrographs of MDA-MB-231 cells (A, B, C) and MCF-7 cells (D, E, F) after 3, 6 and 24 h treatment with QDs. White squares mark the zoomed parts shown in the inserts. Inserts' scale bar=1 μm. The red color shows QDs, the green color – actin staining, the blue color – nucleus staining.G – diameter of vesicles inside MCF-7 and MDA-MB-231 cells, evaluated by image analysis of micrographs.
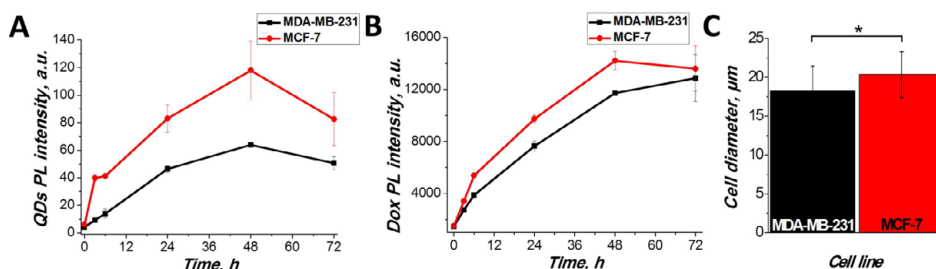
Figure 3: Accumulation dynamics of QDs (A) and doxorubicin (B) in MDA-MB-231 and MCF-7 cells. Cells were incubated with non-targeted QDs or doxorubicin for 3-72 h, trypsinized and analyzed by flow cytometer. C – diameter of MDA-MB-231 and MCF-7 cells. The diameter of trypsinized cells was measured by phase contrast microscopy. More than 20 cells per sample were counted to get the reportable results. Asterisk (*) indicates statistical significance by two-tailed Student's t test ($p < 0.05$).
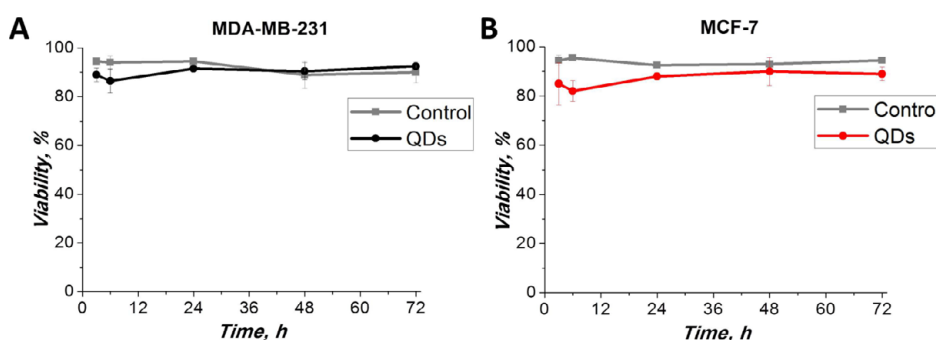

Figure 4: Viability of MDA-MB-231 (A) and MCF-7 (B) cells after the treatment with QDs. After 3-72 h incubation with non-targeted QDs cells were trypsinized and their viability was measured using automated cell counter ADAM.

weak signal of anti-CD44-QDs was registered in the plasma membrane of MCF-7 cells. On the contrary, strong labeling was registered in the MDA-MB-231 cells: after 30 min incubation anti-CD44-QDs brightly and continuously labeled the plasma membrane of cells (Figure 5B). To elucidate the fate of membrane-bound anti-CD44-QD, labeled cells were kept under standard culture conditions (37°, 5% CO_2) for 24 hours. After 24 hours, redistribution was registered in the anti-CD44-QD-labeled cells: anti-CD44-QDs conjugates were engulfed and packed into vesicles (Figures 5E and 5F) similarly to the behavior of non-targeted QDs in cells (Figures 2A-2F).

To clarify whether anti-CD44-QDs engulfment was conditioned by receptor-mediated endocytosis [39], the analogous experiment was carried out in cells using anti-CD44 conjugated to FITC. As expected, the micrographs of MCF-7 cells showed a weak signal of anti-CD44-FITC (Figure 5C) and a strong labeling of the membrane of MDA-MB-231 cells (Figure 5D). After 24 hours under standard culture conditions (37°, 5% CO_2), the bulk of anti-CD44-FITC still remained on the cell surface with a few vesicles inside the cells, indicating the absence of receptor-mediated endocytosis (Figures 5G and 5H).

Discussion

CD44 molecule has been investigated as a potential therapeutic target in oncological diseases since 1990s. CD44 and its splice variants correlated with poor prognosis in breast cancer [40], colorectal cancer [41], high-grade non-Hodgkin's lymphoma [42], gastric [43] and cervical cancers [44]. Later CD44 expression was associated with migration, metastasis, and therapy-resistance of cancer stem-like cells [8,45,46]; therefore CD44 became a crucial target for tumor therapy in many types of cancer. The first clinical trials using anti-

CD44 antibodies showed a 10% response rate [47], thus encouraging scientists to develop a new class of targeted compounds – anti-CD44-nanoparticle conjugates.

In this study we used two human breast cancer cell lines to determine uptake of non-targeted and anti-CD44-conjugated QDs in distinct phenotypic profiles of breast cancer. MDA-MB-231 cells demonstrated >97% of CD44+/CD24-/EpCAM+ cells, effective formation of colonies, and over 2 times lower doxorubicin sensitivity in comparison to MCF-7 cells (Figure 1). Numerous studies showed that CD44+/CD24- cells, found in breast tumors and cell lines, possess cancer stem-like properties [8,28,34,48]. MCF-7 cells demonstrated >93% of CD44low/-/CD24+/EpCAM+ cells. CD44low/-/CD24+cells exhibit features of more differentiated luminal epithelial cells [34].

The majority of current drug carriers are made of polymers and fewer are based on inorganic materials. A common limitation shared by polymeric delivery vehicles is the lack of an intrinsic signal for long-term and real-time imaging of drug transport [49]. In this context, QDs became a natural choice because of their unique spectral properties. Attachment of antibodies [50] and photosensitizers [22] enables development of QDs potentially suitable for selective imaging and eradication of cancer stem-like cells. Antibody-mediated targeted delivery systems represent a powerful new therapeutic approach that could significantly enhance delivery efficacy and minimize toxicity. However, targeted nanoparticles must simultaneously overcome multiple challenges, including selective binding to the target cells and entrance inside them. Our results showed that non-targeted QDs accumulate in the cytoplasm of cancer cells of both phenotypes in vesicular structures (Figure 2), but in MCF-7 cells the PL intensity of QDs was ~ 2.4 times higher than in MDA-MB-231 cells (Figure
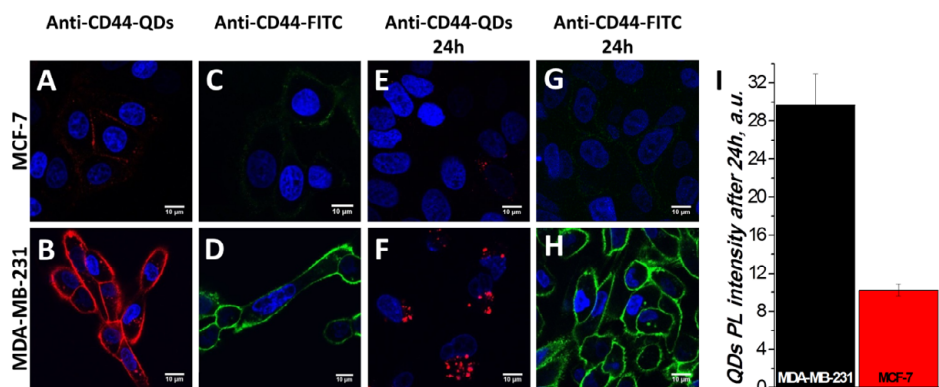
Figure 5: Uptake of anti-CD44-conjugated QDs and anti-CD44-conjugated FITC in breast cancer cells. Fluorescence confocal micrographs of living MCF-7 and MDA-MB-231 cells were taken at two time-points: immediately after treatment with anti-CD44-QD (A, B) and anti-CD44-FITC (C, D), and at 24 h post treatment (E, G, F, H). The red color shows anti-CD44-QDs, the green color – anti-CD44-FITC staining, the blue color – nucleus staining. I-Quantitative QDs intensities from E and F. Cells from each image were randomly selected to calculate mean values ± SD.

3A). PL intensity indicates the number of nanoparticles inside cells; therefore, higher PL intensity might be related to better uptake of QDs in $CD44^{low/-}/CD24^+/EpCAM^+$ cells in comparison to $CD44^+/CD24^-/EpCAM^+$. Cell-type related difference in QDs uptake was also registered in our previous study: although the distribution of non-targeted QDs followed similar accumulation stages and morphological phases in three distinct cell lines, the PL intensity of QDs within one cell was highest in MCF-7 cells [35]. The main explanation could be the different physiology of the cell lines and cell type-specific surface receptors [51].

We also evaluated the diameter of QD-packed vesicles in both cell lines. While MCF-7 cells showed gradual enlargement in vesicles during incubation time, ending up with 1 μm diameter at 24 hours, MDA-MB-231 cells demonstrated the presence of vesicles over 3 μm in diameter at the initial time point (3 hours) (Figure 2G). Rak-Raszewska et al. investigated uptake of QDs in kidney stem cells and also found heterogeneous distribution of vesicles; over 2 times difference in vesicle diameter inside the same cell [52]. Another study investigated QDs uptake in migrating MDA-MB-231 cells and also found large vesicles of QDs inside these cells [53]. The reason for enlarged vesicle formation is still unknown but there are studies showing that mutation and dysfunction of Rab5 protein, involved in early endosome formation, induces the enlargement of the vesicles and causes their fusion [54].

Antibody-conjugated nanoparticles were shown to effectively deliver drugs or genes to targeted cells by specifically binding to the antigens that are exposed on the targeted cells surface [51]. However, the information about localization and cellular distribution of those conjugates is still missing. For cellular distribution studies we used laser scanning confocal imaging of living cells to specifically monitor the fate of anti-CD44-QDs and anti-CD44-FITC conjugates in MDA-MB-231 and MCF-7 cells, which represent $CD44^+/CD24^-/EpCAM^+$ and $CD44^{low/-}/CD24^+/EpCAM^+$ phenotypes, respectively. Only slight binding of anti-CD44-QDs to the membrane of MCF-7 cells was detected, while the membrane of MDA-MB-231 cells was brightly and continuously labeled within 30 min (Figure 5). Most interestingly, within 24 hours post incubation, membrane-bound anti-CD44-QDs were completely engulfed inside the cells and packed into the vesicles. MDA-MB-231 cells in parallel were labeled with anti-CD44-FITC conjugates but minimal engulfment was registered after 24 h. The engulfment of anti-CD44-QDs inside cells shows the capability of QDs

to not only selectively label CD44+ cells, but also shows a potential to transport molecules inside cancer cells. It is unknown why antibody-conjugated QDs were endocytosed, while organic molecule FITC-conjugated antibodies remained on the plasma membrane. The size of the QD might be a determinant of endocytosis as it resembles the size of CD44 ligand hyaluronic acid [39], but further studies are needed to give a reasonable explanation.

Conclusion

Combining molecular probes such as quantum dots with anti-CD44 antibodies, we were able to initiate engulfment of membrane bound anti-CD44-QDs. To our knowledge, this is the first time when antibody-conjugated quantum dots were selectively engulfed inside CD44+ cells. The most important finding is the synergistic effect of the conjugate: anti-CD44 is capable of target recognition and quantum dot is capable of endocytosis initiation. We suggest that conjugates of antibodies and photoluminescent nanoparticles should be used in the development of multifunctional agents for selective labeling and therapy of cancer.

Acknowledgement

References

1. Goldthwaite CA (2006) Are stem cells involved in cancer? In: Regenerative medicine, (Ed.^(Eds). 89-95.

2. Baumann M, Krause M, Hill R (2008) Exploring the role of cancer stem cells in radioresistance. Nature reviews. Cancer 8: 545-554.

3. An Y, Ongkeko WM (2009) ABCG2: The key to chemoresistance in cancer stem cells? Expert opinion on drug metabolism and toxicology 5: 1529-1542.

4. Al Dhaybi R, Sartelet H, Powell J, Kokta V (2010) Expression of CD133+ cancer stem cells in childhood malignant melanoma and its correlation with metastasis. Mod Pathol 23: 376-380.

5. De Beca FF, Caetano P, Gerhard R, Alvarenga CA, Gomes M, et al. (2013) Cancer stem cells markers CD44, CD24 and ALDH1 in breast cancer special histological types. Journal of clinical pathology 66: 187-191.

6. Chen K, Huang YH, Chen JL (2013) Understanding and targeting cancer stem cells: Therapeutic implications and challenges. Acta pharmacologica Sinica 34: 732-740.

7. Orian-Rousseau V (2010) CD44, a therapeutic target for metastasising tumours. Eur J Cancer 46: 1271-1277.

8. Al-Hajj M, Wicha MS, Benito-Hernandez A, Morrison SJ, Clarke MF (2003) Prospective identification of tumorigenic breast cancer cells. P Natl Acad Sci USA 100: 3983-3988.

9. Hurt EM, Kawasaki BT, Klarmann GJ, Thomas SB, Farrar WL (2008) CD44(+) CD24(-) prostate cells are early cancer progenitor/stem cells that provide a model for patients with poor prognosis. Brit J Cancer 98:756-765.

10. Li CW, Heidt DG, Dalerba P, Burant CF, Zhang L, et al. (2007) Identification of pancreatic cancer stem cells. Cancer Res 67: 1030-1037.

11. Kozovska Z, Gabrisova V, Kucerova L (2014) Colon cancer: Cancer stem cells markers, drug resistance and treatment. Biomed Pharmacother 68: 911-916.

12. Athanassiou-Papaefthymiou M, Shkeir O, Kim D, Divi V, Matossian M, et al. (2014) Evaluation of CD44 variant expression in oral, head and neck squamous cell carcinomas using a triple approach and its clinical significance. Int J Immunopath Ph 27: 337-349.

13. Wang LN, Su WJ, Liu Z, Zhou M, Chen S, et al. (2012) CD44 antibody-targeted liposomal nanoparticles for molecular imaging and therapy of hepatocellular carcinoma. Biomaterials 33: 5107-5114.

14. Han XP, Li ZB, Sun J, Luo C, Li L, et al. (2015) Stealth CD44-targeted hyaluronic acid supramolecular nanoassemblies for doxorubicin delivery: Probing the effect of uncovalent pegylation degree on cellular uptake and blood long circulation. J Control Release 197: 29-40.

15. Nejadnik MR, Yang X, Bongio M, Alghamdi HS, van den Beucken JJ, et al. (2014) Self-healing hybrid nanocomposites consisting of bisphosphonated hyaluronan and calcium phosphate nanoparticles. Biomaterials 35: 6918-6929.

16. Zhao YQ, Zhang T, Duan SF, Davies NM, Forrest ML (2014) CD44-tropic polymeric nanocarrier for breast cancer targeted rapamycin chemotherapy. Nanomed-Nanotechnol 10: 1221-1230.

17. Melancon MP, Zhou M, Li C (2011) Cancer theranostics with near-infrared light-activatable multimodal nanoparticles. Accounts of chemical research 44: 947-956.

18. Zrazhevskiy P, Sena M, Gao X (2010) Designing multifunctional quantum dots for bioimaging, detection, and drug delivery. Chemical Society reviews 39: 4326-4354.

19. Alivisatos AP, Gu W, Larabell C (2005) Quantum dots as cellular probes. Annual review of biomedical engineering 7: 55-76.

20. Smith AM, Duan H, Mohs AM, Nie S (2008) Bioconjugated quantum dots for in vivo molecular and cellular imaging. Advanced drug delivery reviews 60: 1226-1240.

21. Juzenas P, Chen W, Sun YP, Coelho MA, Generalov R, et al. (2008) Quantum dots and nanoparticles for photodynamic and radiation therapies of cancer. Advanced drug delivery reviews 60: 1600-1614.

22. Steponkiene S, Valanciunaite J, Skripka A, Rotomskis R (2014) Cellular uptake and photosensitizing properties of quantum dot-chlorin e(6) complex: In vitro study. J Biomed Nanotechnol 10: 679-686.

23. Yang K, Zhang FJ, Tang H, Zhao C, Cao YA, et al. (2011) In-vivo imaging of oral squamous cell carcinoma by egfr monoclonal antibody conjugated near-infrared quantum dots in mice. International journal of nanomedicine 6: 1739-1745.

24. Cai W, Shin DW, Chen K, Gheysens O, Cao Q, et al. (2006) Peptide-labeled near-infrared quantum dots for imaging tumor vasculature in living subjects. Nano letters 6: 669-676.

25. Jennings TL, Becker-Catania SG, Triulzi RC, Tao G, Scott B, et al. (2011) Reactive semiconductor nanocrystals for chemoselective biolabeling and multiplexed analysis. ACS nano 5: 5579-5593.

26. Kelf T, Sreenivasan V, Sun J, Kim E, Goldys E, Zvyagin A (2010) Non-specific cellular uptake of surface-functionalized quantum dots. Nanotechnology 21: 285105.

27. Sheridan C, Kishimoto H, Fuchs RK, Mehrotra S, Bhat-Nakshatri P, et al. (2006) CD44(+)/CD24(-) breast cancer cells exhibit enhanced invasive properties: An early step necessary for metastasis. Breast Cancer Res 8.

28. Yin H, Glass J (2011) The phenotypic radiation resistance of CD44(+)/CD24(-or) (low) breast cancer cells is mediated through the enhanced activation of atm signaling. Plos One 6.

29. Zheng XS, Shen G, Yang XF, Liu WG (2007) Most c6 cells are cancer stem cells: Evidence from clonal and population analyses. Cancer Res 67: 3691-3697.

30. Liu TI, Sun BC, Zhao XL, Zhao XM, Sun T, et al. (2013) CD133(+) cells with cancer stem cell characteristics associates with vasculogenic mimicry in triple-negative breast cancer. Oncogene 32: 544-553.

31. Beaver CM, Ahmed A, Masters JR (2014) Clonogenicity: Holoclones and meroclones contain stem cells. Plos One 9.

32. Chuthapisith S, Eremin J, El-Sheemey M, Eremin O (2010) Breast cancer chemoresistance: Emerging importance of cancer stem cells. Surg Oncol 19: 27-32.

33. Kalluri R, Weinberg RA (2009) The basics of epithelial-mesenchymal transition. J Clin Invest 119: 1420-1428.

34. Fillmore CM, Kuperwasser C (2008) Human breast cancer cell lines contain stem-like cells that self-renew, give rise to phenotypically diverse progeny and survive chemotherapy. Breast Cancer Res 10.

35. Damalakiene L, Karabanovas V, Bagdonas S, Valius M, Rotomskis R (2013) Intracellular distribution of nontargeted quantum dots after natural uptake and microinjection. Int J Nanomed 8: 555-568.

36. Karabanovas V, Zitkus Z, Kuciauskas D, Rotomskis R, Valius M (2014) Surface properties of quantum dots define their cellular endocytic routes, mitogenic stimulation and suppression of cell migration. J Biomed Nanotechnol 10: 775-786.

37. Damalakiene L, Karabanovas V, Bagdonas S, Pupelis L, Valius M, et al. (2015) Suppression of a specific intracellular uptake pathway by a saturating accumulation of quantum dots. J Biomed Nanotechnol 11: 841-853.

38. Zhang LV, Monteiro-Riviere NA (2009) Mechanism of quantum dot nanoparticle cellular uptake. Toxicological sciences: an official journal of the Society of Toxicology 110: 138-155.

39. Racine R, Mummert ME (2012) Hyaluronan endocytosis: Mechanisms of uptake and biological functions. In: Molecular regulation of endocytosis, (Ed.^(Eds). 378-390.

40. Joensuu H, Klemi PJ, Toikkanen S, Jalkanen S (1993) Glycoprotein CD44 expression and its association with survival in breast cancer. Am J Pathol 143: 867-874.

41. Wielenga VJM, Van Der Neut R, Offerhaus GJA, Pals ST (2000) CD44 glycoproteins in colorectal cancer: Expression, function, and prognostic value. Advances in Cancer Research 77 77: 169-187.

42. Stauder R, Eisterer W, Thaler J, Gunthert U (1995) CD44 variant isoforms in non-hodgkin's lymphoma: A new independent prognostic factor. Blood 85: 2885-2899.

43. Hsieh HF, Yu JC, Lo LI, Chiu SC, Harn HJ (1999) Molecular studies into the role of CD44 variants in metastasis in gastric cancer. J Clin Pathol-Mol Pa 52: 25-28.

44. Kainz C, Kohlberger P, Tempfer C, Sliutz G, Gitsch G, et al. (1995) Prognostic value of CD44 splice variants in human stage III cervical cancer. Eur J Cancer 31A: 1706-1709.

45. Steponkiene S, Kavaliauskiene S, Purviniene R, Rotomskis R, Juzenas P (2011) Quantum dots affect expression of CD133 surface antigen in melanoma cells. Int J Nanomedicine 6: 2437-2444.

46. Ni J, Cozzi PJ, Hao JL, Beretov J, Chang L, et al. (2014) CD44 variant 6 is associated with prostate cancer metastasis and chemo-/radioresistance. Prostate 74: 602-617.

47. Riechelmann H, Sauter A, Golze W, Hanft G, Schroen C, et al. (2008) Phase I trial with the CD44v6-targeting immunoconjugate bivatuzumab mertansine in head and neck squamous cell carcinoma. Oral Oncol 44: 823-829.

48. Phuc PV, Phan LCN, Nhung TH, Tam NT, Hoang NM, et al. (2011) Downregulation of CD44 reduces doxorubicin resistance of CD44(+)CD24(-) breast cancer cells. Oncotargets Ther 4: 71-78.

49. Qi LF, Gao XH (2008) Emerging application of quantum dots for drug delivery and therapy. Expert Opin Drug Del 5: 263-267.

50. Tiwari DK, Tanaka S, Inouye Y, Yoshizawa K, Watanabe TM, et al. (2009) Synthesis and characterization of anti-HER2 antibody conjugated CdSe/CdZnS quantum dots for fluorescence imaging of breast cancer cells. Sensors 9: 9332-9364.

51. Douglas KL, Piccirillo CA, Tabrizian M (2008) Cell line-dependent internalization pathways and intracellular trafficking determine transfection efficiency of nanoparticle vectors. Eur J Pharm Biopharm 68: 676-687.

52. Rak-Raszewska A, Marcello M, Kenny S, Edgar D, See V, et al. (2012) Quantum dots do not affect the behaviour of mouse embryonic stem cells and kidney stem cells and are suitable for short-term tracking. Plos One 7: e32650.

53. Parak WJ, Boudreau R, Le Gros M, Gerion D, Zanchet D, et al. (2002) Cell motility and metastatic potential studies based on quantum dot imaging of phagokinetic tracks. Adv Mater 14: 882-885.

54. Shimizu H, Kawamura S, Ozaki K (2003) An essential role of Rab5 in uniformity of synaptic vesicle size. J Cell Sci 116: 3583-3590.